# Two-matrix composites: Carbon fiber micropultrusions embedded in flexible epoxy matrices

Callens, Sebastien; Bergsma, Otto

**DOI**
10.1016/j.compositesa.2018.08.008

**Publication date**
2018

**Document Version**
Accepted author manuscript

**Published in**
Composites Part A: Applied Science and Manufacturing

# Accepted Manuscript


Two-matrix Composites: Carbon Fiber Micropultrusions Embedded in Flexible Epoxy Matrices

Sebastien J.P. Callens, Otto K. Bergsma

PII: S1359-835X(18)30318-X
DOI: https://doi.org/10.1016/j.compositesa.2018.08.008
Reference: JCOMA 5142

To appear in: *Composites: Part A*

Received Date: 9 February 2018
Revised Date: 3 May 2018
Accepted Date: 9 August 2018

Please cite this article as: Callens, S.J.P., Bergsma, O.K., Two-matrix Composites: Carbon Fiber Micropultrusions Embedded in Flexible Epoxy Matrices, *Composites: Part A* (2018), doi: https://doi.org/10.1016/j.compositesa.2018.08.008

# Two-matrix Composites: Carbon Fiber Micropultrusions Embedded in Flexible Epoxy Matrices

Sebastien J.P. Callens*, Otto K. Bergsma

*Department of Aerospace Structures and Materials, Delft University of Technology (TU Delft), Kluyverweg 1, 2629 HS Delft , The Netherlands.*

**ABSTRACT**

Two-matrix composites combine fibers with two distinct matrices. This is achieved by impregnating fiber bundles with a high-stiffness matrix and embedding the cured bundles in a flexible matrix. Two-matrix composites have been shown to offer unprecedented combinations of transverse flexibility and longitudinal tensile strength, and could offer improved fiber alignment and manufacturability. Here, we explore this concept further by embedding carbon fiber micropultrusions in flexibilized epoxy matrices and examining the longitudinal compression behavior. Our results on thin-walled rings reveal that the failure mode depends on micropultrusion diameter, with small diameters resulting in micropultrusion kinking and larger diameters in splitting and crushing. Additionally, we find that two-matrix composites can offer higher compression strength than conventional composites with the same flexible matrix, despite a lower fiber volume fraction. The inherent manufacturing advantages and high anisotropy could make two-matrix composites interesting candidates for specific applications, such as morphing wings or additively manufactured composites.

**Keywords:** Mechanical testing (D), Filament winding (E), Mechanical properties (B), Transverse cracking (B)

* corresponding author: s.j.p.callens@tudelft.nl

## 1. INTRODUCTION

Several high-performance industries have adopted the use of continuous fiber-reinforced polymer composites (FRPCs) for structural components in recent decades. Typically, the fundamental building block of these composite structures is the unidirectional (UD) composite layer. A classical UD layer consists of many fibers, typically carbon, that are arranged in one single direction and are embedded in a polymer matrix, most commonly a thermoset. One particularly limiting characteristic of a typical UD layer is the low tensile failure strain in transverse direction $\bar{\epsilon}_{t,2}$, as compared to that in longitudinal direction $\bar{\epsilon}_{t,1}$. For a typical UD carbon fiber epoxy composite, the longitudinal tensile failure strain would be approximately 1.5%, while the transverse tensile failure strain would remain below 1% [1, 2]. This anisotropy in terms of tensile failure strain is problematic for composite laminates, in which all layers are expected to strain by the same amount when the laminate is uniaxially loaded. Tensile loading of a laminate along one direction could result in matrix cracks in the off-axis plies, due to the mismatch between $\bar{\epsilon}_{t,1}$ and $\bar{\epsilon}_{t,2}$ (see Figure 1a). Such transverse matrix cracks negatively affect the performance of the composite laminate as they could degrade the thermomechanical properties of the laminate, initiate delamination damage, and facilitate moisture ingress [3-5]. In attempt to solve this problem, Vasiliev and Salov proposed a radically different type of unidirectional composite, in which fibers are combined with two distinct matrix materials, instead of only one matrix [6]. In their "two-matrix" composites, glass fiber bundles were first impregnated with a high-stiffness epoxy matrix and cured, after which the composite bundles were embedded in a secondary, flexible epoxy matrix that would provide the composite with high transverse flexibility (Figure 1b). The "direct" solution of embedding standard fibers in a flexible matrix was found to be unfeasible since the increase in transverse flexibility, achieved by selecting a highly flexible matrix, would come at the unacceptable cost of a significant reduction in longitudinal tensile strength (Table 1).

This is because the flexible matrix is less efficient at transferring stress between fibers around fiber breaks. Two-matrix composites offer a better route, as they separate the two conflicting functions of the matrix between two different matrix materials. The stiff matrix provides efficient stress transfer around fiber breaks and results in a high longitudinal strength, while the flexible matrix enables a high transverse tensile failure strain.

While Vasiliev and Salov were the first to propose the two-matrix concept for combating low transverse flexibility of UD composites, other researchers have investigated similar ideas. In the "Design and Manufacture of Low-Cost Composite-Bonded Wing" program, an improved and cost-efficient stiffening approach for hat stiffeners was sought [7]. The proposed solution consisted of embedding pultruded rod packs in a syntactic adhesive, which was shown to offer reduced manufacturing cost and complexity without suffering reductions in structural efficiency, in part due to the low fiber waviness [8]. Potter and Wisnom [9] proposed "composites of extreme anisotropy" for applications requiring both a high bending stiffness and a low torsional rigidity. Similarly to the work of Vasiliev and Salov, the researchers embedded carbon fiber pultruded rods (1.7mm diameter) in a low-stiffness matrix and performed mechanical tests. The researchers could successfully achieve high bending-to-shear stiffness ratios and showed that a demonstrator beam could withstand twist angles up to 20° without signs of permanent damage. Cairns and Bundy [10] suggested the use of carbon fiber pultruded rods (1.2mm diameter) embedded in a secondary (non-flexible) epoxy matrix to reduce carbon fiber waviness in wind turbine blade applications. The researchers experimentally investigated the effect of surface treatments on the interfacial shear strength between the rods and the surrounding epoxy matrix, and found the highest strength values for media blast erosion. A final comparable concept was presented by Schmitz and Horst [11], who embedded composite bundles in an elastomeric foundation to develop a morphing wing skin with adequate span-wise bending stiffness. The researchers performed compression

experiments and FEA, and observed buckling of the bundles inside the compliant foundation. However, the bundles used by Schmitz and Horst [11] had an elliptical cross section with a major axis of 2mm and were made by stacking strips of carbon fiber prepreg. Additionally, the compliant foundation was supported on one side by a composite laminate, which would not be the case in a general two-matrix composite. An important difference of all these examples with the two-matrix composites of Vasiliev and Salov [6], is the considerably larger bundle diameter: 1.2mm-2mm as opposed to approximately 0.5mm. The use of small diameter bundles enabled the researchers to directly swap the fiber tows with the composite bundles in their manufacturing process. Nonetheless, these examples indicate other potential advantages of the use of pre-cured bundles embedded in a secondary matrix, such as reduced manufacturing costs or increased fiber alignment. As such, it is interesting to explore the two-matrix concept further and to investigate whether it could lead to an alternative building block for the design of composite structures. Here, we present our own type of two-matrix composite, consisting of carbon fiber micropultrusions embedded in a flexibilized epoxy matrix. Our work is the first (to our knowledge) to combine such small diameter pultrusions (280 $\mu m$ – 700 $\mu m$ diameter) in a secondary, flexible matrix, synthesized using only epoxy resins and appropriate hardener. We discuss the selection and synthesis of the constituent materials, as well as the manufacturing method to create two-matrix composites. In the same spirit as the work of Vasiliev and Salov [6], we use a manufacturing set-up where the input material could easily switch between fiber tows and pre-cured composite bundles. Moreover, we build upon the earlier foundations in terms of longitudinal and transverse tensile strength, and further explore the mechanical performance. We focus here on the longitudinal compression strength, as this property is often a critical design driver for high-performance composite structures [12]. While some of the abovementioned similar works have also considered the compression response, e.g. Potter and Wisnom [9], and Schmitz and Horst

[11], we perform a different type of compression test in order to prevent global specimen buckling and we explore the influence of both flexible matrix stiffness and micropultrusion diameter on the compression strength.

## 2. MATERIALS & METHODS

### 2.1 Carbon fiber micropultrusions

The two primary constituents of a two-matrix composite are the composite bundles, consisting of fibers embedded in a stiff matrix, and the flexible matrix surrounding these bundles. In their earlier work, Vasiliev and Salov constructed composite bundles by impregnating and curing a dry bundle of 500 glass fiber filaments with an epoxy matrix [6]. While these researchers reported high fiber volume fractions and successful bundle implementation in the flexible matrix, the cross-sectional micrographs of the bundles revealed inconsistent cross-sectional shapes and the presence of relatively large voids [1]. To improve on this, we employed state-of-the art carbon fiber *micropultrusions*, i.e. small-diameter pultruded rods, with circular cross sections (Figure 2). We obtained three types of micropultrusions from a commercial manufacturer (vDijk Pultrusion Products (DPP), the Netherlands [13]) with diameters of $280\mu m$, $500\mu m$ and $700\mu m$. All micropultrusions were manufactured from Torayca T300 carbon fibers (Toray Industries, Japan), using 1K, 3K and 6K tows for the $280\mu m$, $500\mu m$ and $700\mu m$ diameters respectively. The fiber volume content for all micropultrusions was between 60-65%. In case of the $280\mu m$ diameter micropultrusions, a bismaleimide (BMI) matrix was used ($E = 4.6$ GPa, $\epsilon_{ult} = 4.8\%$ according to specification) while an epoxy matrix was used for the other two types ($E = 3.3$ GPa, $\epsilon_{ult} = 7\%$ according to specification). The difference in matrix type was due to the availability and production set-up at the time of acquisition (280 $\mu$m micropultrusions with epoxy could not be made available in due time). However, this was not expected to cause significant differences on the test results, since the stiffness of both matrices was considerably higher than the stiffness of

the flexible matrix in which they were embedded. Additionally, the difference in matrix stiffness would cause only a minor change in micropultrusion bending stiffness (and thus resistance against potential buckling), while the micropultrusion diameter would play a much more significant role. Micropultrusions are typically used in biomedical applications [14] and are characterized by a high fiber volume fraction, accurate control over the cross-sectional shape, excellent fiber alignment and a high overall quality. The selected micropultrusions are displayed in Figure 2, both in a straight and curved configuration. As compared to a dry fiber tow, a micropultrusion has a noticeable bending stiffness, which naturally increases for larger diameters. Despite this inherent bending stiffness and tendency to straighten, all three types of micropultrusions could withstand relatively high curvatures. Figure 2 also shows a cross-sectional micrograph of a $280\mu m$ micropultrusion, showing the circular cross section, the uniform distribution of fibers throughout the cross-section and the high fiber volume fraction.

**2.2 Flexibilized epoxy matrix**

The flexible matrix in which the micropultrusions are embedded is the second major constituent of two-matrix composites. By considering aspects such as mechanical performance, processing characteristics and the compatibility with the micropultrusions, a *flexibilized epoxy matrix* was selected during this research, obtained by blending different ratios of a standard epoxy resin based on diglycidyl ether of bisphenol A (EPIKOTE EPH 04908, Hexion, USA) with a bisphenol A-based monofunctional, aliphatic epoxy resin (EBL 1435, EP Plus, Belgium). The addition of this second, flexibilizing component resulted in longer polymer chains and a lower overall cross-link density, thereby lowering the stiffness of the cured epoxy system below the values of typical epoxy systems. The resin blend was cured using an amine-based hardener (EPIKURE EPR 04908, Hexion, USA). The stoichiometric ratio of hardener to resin was determined based on the amine equivalent weight (AEW) of the hardener and the epoxy equivalent weight (EEW) of both epoxy resins. While a number of

other flexibilizing strategies also exist, such as the addition of elastomers (this was used in the work of Vasiliev and Salov [6]), thermoplastic polymers, or non-reactive plasticizers, the strategy based on blending or "alloying" of different epoxy resins [15], enabled us to use straightforward processing techniques to synthesize the flexible matrix and manufacture the two-matrix composites.

Naturally, combining the standard epoxy resin with the flexibilizing resin in various ratios would result in a varying degree of matrix stiffness. The effect of the flexibilizing resin on the matrix stiffness was quantified using three-point flexural testing of cured epoxy specimens, in accordance with test standard ASTM D790. Trial experiments revealed that quantities of flexibilizing resin below 40% of the total resin content did not result in a significant stiffness reduction, while quantities above 70% resulted in specimens that were too flexible for testing with the three-point bending set-up. Figure 3a shows the flexural stiffness results for the standard epoxy matrix without flexibilizer, as well as three flexibilized matrices that were selected for further use within this research. Additional data is provided in Table 2. The matrix with a stiffness of 0.7 $GPa$ was selected as the baseline matrix for the development of two-matrix composites within this research. Further characterization of this flexible baseline matrix was performed using tensile testing and dynamic mechanical analysis (DMA) on cured epoxy specimens. The tensile tests were performed on dogbone specimens (milled from cured epoxy plates), in accordance with test standard ASTM D638. Figure 3b shows two typical stress-strain curves for the cured flexible baseline matrix and for the standard matrix without flexibilizer. Clearly, the addition of the flexibilizer not only reduces the elastic stiffness, but also results in a significant increase in tensile failure strain (from an average of 2.5% for the standard matrix to an average of 35.4% for the flexible baseline matrix, see also Table 2). The glass transition temperature ($T_g$) of the flexible baseline matrix was determined using a DMA in three-point bending mode. As shown in Table 2, the onset of $T_g$ occurred at $37°C$ (peak of

the loss modulus $E''$), while the "average" $T_g$ was situated at $57°C$ (peak of the tan($\delta$) curve). Indeed, the addition of the flexibilizer entails a reduction in $T_g$ as compared to the unflexibilized matrix ($T_g = 82°C$), which is a consequence of the reduced cross-link density. Nevertheless, the glass transition temperature of the flexible baseline matrix was deemed sufficiently high to enable testing at ambient laboratory temperatures.

**2.3 Manufacturing of ring specimens**

In order to evaluate the mechanical performance of the two-matrix composites and compare it to that of standard (single-matrix) composites, we manufactured thin-walled ring specimens using filament winding. Compared to other manufacturing strategies, filament winding offered the advantage that the bobbins on which the continuous micropultrusions were delivered could be directly used as input materials to the winding machine. In terms of testing, the use of rings was deemed advantageous since these specimens do not suffer from undesired end failure or clamping issues as standard rectangular specimens do. In rectangular specimens, the load introduction at the ends of the specimens is often problematic, in particular for compression testing of UD composites. In case of composites with a flexible matrix, this load introduction into the specimens could be even more challenging, since partial load transfer due to shear might not be possible [11]. As such, ring specimens were considered a more reliable choice for evaluating the compression strength of two-matrix composites. The specimen dimensions were defined such that the rings would classify as being thin-walled, meaning that the ratio of ring radius to wall thickness would exceed 20 (in our case: $\frac{R_{in}}{t} = 25$) [16]. The dimensions of the composite rings used during this research are given in Figure 4a. All composite specimens were manufactured on a tailor-made cylindrical mandrel that was assembled from a central aluminum cylinder and seven equally spaced, plastic rings made from low-adhesion polyoxymethylene (POM). The equal spacing of the plastic rings provided six slots in which the composite rings could be wound, enabling the

manufacturing of six composite rings during every production cycle (Figure 4b). Both the single- and two-matrix composites were manufactured using a wet filament winding process, although variations between both cases were present due to the different types of reinforcement (standard fibers versus micropultrusions). In case of the single-matrix specimens, a 12K T300 carbon fiber tow was installed on a fiber tension unit and pulled through a resin bath prior to being wound on the mandrel, in order to align the fibers within the tow and to enable resin migration into the tow. The two-matrix composites, on the other hand, did not require tensioning of the micropultrusions nor was it necessary to pull them through a resin bath, since the micropultrusions already consisted of highly aligned fibers and because there was no need for matrix migration *into* the micropultrusion. Instead, the flexible matrix merely needed to surround the micropultrusions, which was achieved by directly depositing the flexible matrix in the mandrel slots during winding. Due to the simplified manufacturing lay-out and the easier impregnation, the production cycle (without curing) for a set of two-matrix composites (2-4 hours) was considerably shorter than for single-matrix composites (6 hours). Upon completion of the winding process, the entire mandrel was installed in an oven on a rotating drum, and fully cured for 12 hours at 80°C. The same curing cycle was used for all specimens. After the curing cycle and the subsequent cool-down phase, the mandrel was disassembled and the composite rings were demolded from the aluminum cylinder and were carefully trimmed to remove excess matrix material.

**2.4 Ring compression test**

Different compression test methods for hoop-wound ring specimens have been developed in the past decades. The general idea of these methods is to apply a radial compression force along the circumference, inducing hoop and radial stresses in the rings [17]. When a thin-walled ring is tested, however, the radial stress is negligible and the hoop stress is nearly constant throughout the ring thickness. Hence, for thin-walled, hoop-wound rings, these test

methods could be used to determine the longitudinal compression strength [16]. Here, we used a relatively simple, yet very effective test method that was first proposed by Kim and Tsai [18]. In this method, a composite ring is placed inside a larger, rubber ring (42 Shore-A hardness), which is on its turn confined on the outer surface by a steel base. During testing, the rubber ring is axially compressed by a loading plate, resulting in radial expansion inwards (due to Poisson's effect), thereby exerting a radial compression force on the composite ring (see Figure 5). Since rubber behaves as a nearly incompressible material ($\nu \approx 0.5$), axial compression of the confined rubber ring results in a near-perfect hydrostatic pressure build-up [19]. The set-up was used for compression testing of both single- and two-matrix composite rings, following the same procedure. Every composite ring was equipped with four, equally spaced strain gauges that were attached to the inner wall of the ring. The entire set-up was installed in between two compression plates on a 500 kN test bench and a pre-load of 500 N was applied. The test itself was displacement controlled (1 mm/min) and the test bench load and displacement were continuously recorded, as was the strain of the four strain gauges. The rings were loaded until failure, which occurred abruptly in all cases. In order to convert the measured test bench force to the hoop stress ($\sigma_h$) and radial stress ($\sigma_r$) in the composite rings, we employed the expressions provided by Lekhnitskii [20]:

$$\sigma_h = \frac{-qk}{1-c^{2k}}\left(\left(\frac{r}{R_{out}}\right)^{k-1} + c^{2k}\left(\frac{R_{out}}{r}\right)^{k+1}\right)$$

$$\sigma_r = -\frac{q}{1-c^{2k}}\left(\left(\frac{r}{R_{out}}\right)^{k-1} - c^{2k}\left(\frac{R_{out}}{r}\right)^{k+1}\right)$$

These expressions give the stresses as a function of applied pressure ($q$), radial position ($R_{in} \leq r \leq R_{out}$), ring dimensions ($c = R_{in}/R_{out}$) and ring anisotropy ($k = \sqrt{E_{hoop}/E_{radial}}$, where $E_{hoop} = E_1$ and $E_{radial} = E_2$ [18]). As mentioned before, the pressure on the composite rings arises from the axial loading of the rubber ring, and could be calculated as force divided by axial surface area of the ring (due to the hydrostatic pressure build-up in the

rubber ring). Figure 5b shows an example of the stress distribution inside a thin-walled ring with the dimensions used in this research, for an applied pressure of $q = 20MPa$ and an anisotropy ratio of $k = 4.8$. Clearly, the radial stress in the ring is much lower than the hoop stress, both of which are compressive. The radial stress reduces from the applied pressure at the outer surface to zero on the inner surface. The hoop stress, however, is nearly constant throughout the ring thickness at a value of approximately $510\ MPa$, with the maximum reached at the inner surface of the ring. For all the rings tested during this research (with varying matrix stiffness), the $k$-value was estimated to be within the range of $2.6 - 6.3$ (using the Rule of Mixtures for $E_1$ and $\nu_{12}$ and the Halpin-Tsai equations for $E_2$ and $G_{12}$ [21]). Figure 5c shows the ratio of $\sigma_h$ at the inside of the ring to $\sigma_h$ at the outside versus the ratio of inner to outer radius. As can be seen, the highest hoop stress always occurs at the inner surface for the rings used in this research (indicated by the vertical dashed line), independent of the $k$-value. During this research, 33 composite rings were tested in compression. We tested single-matrix composites with the unflexibilized matrix and with the flexible baseline matrix. Furthermore, we tested nine different types of two-matrix composites, all being different combinations of the three flexibilized matrix systems and three micropultrusion diameters. For every category, three repeats were performed.

**2.5 Rectangular specimens**

In addition to the composite rings, UD single-matrix composite plates were also manufactured using vacuum-assisted wet lay-up ($V_f \approx 52\%$). The plates were manufactured from layers of UD carbon fiber fabric (T300) with either the unflexibilized epoxy or with the flexible baseline matrix (68% flexibilizer), i.e. the same materials as those used for the single-matrix composite rings. After curing for 24h at room temperature and 12h at $80°C$, the plates were cut into rectangular specimens. Five specimens with the unflexibilized matrix and five specimens with the flexible baseline matrix were tested in longitudinal compression using the

standard combined loading compression (CLC) test fixture, according to ASTM D6641. Additionally, five specimens of both categories were tested in transverse tension, in accordance with ASTM D3039, to obtain an indication of the transverse flexibility of both composites.

## 3. Results and Discussion

### 3.1 Ring specimen evaluation

Cross-sectional evaluations of the single- and two-matrix composite rings were performed using optical and scanning electron microscopy. Figure 6a displays a typical cross-sectional micrograph of a single-matrix composite specimen. In addition to the high fiber packing density, the micrograph reveals the presence of inter-tow voids, caused by the entrapment of air bubbles in between adjacent fiber tows during the winding process. Using image analysis software (Leica QWin), the fiber and void volume contents were determined for several single-matrix specimens. The average void content was found to be in the range of 2.5-4.1%, which is in line with typical values for the wet filament winding process [22]. The average fiber volume content was determined to be in the range of 50-55%. Figure 6 also displays cross-sectional micrographs of the two-matrix composites, definitely exhibiting a different internal material architecture, with the circular-shaped micropultrusions clearly visible inside the secondary matrix. It is evident from these micrographs that the number of micropultrusions within the cross-section is inversely proportional to the micropultrusion diameter. The cross-sectional evaluations furthermore revealed that all two-matrix composite specimens exhibited variations in micropultrusion packing density (see Figure 6b and Figure 6c), which were attributed to the limited control over the micropultrusion positioning during the winding process. These figures also highlight an important feature of two-matrix composites, namely that material defects arise at a larger scale than for single-matrix composites. For example, the size of the resin pocket in Figure 6c is in the order of the

diameter of a micropultrusions. For single-matrix composites, this would likely be in the order of the diameter of single filaments. Nevertheless, all two-matrix composite specimens exhibited a high overall micropultrusion packing density ($V_b^c$), determined to be within the range of 70-75%. Combining these values with the fiber volume content of the micropultrusions ($V_f^b$=60-65%), the total fiber volume content of the two-matrix composites ($V_f^c$) was conservatively calculated to be within the range of 42-49%. Additionally, the cross-sectional micrographs of all two-matrix composites showed very few signs of voids inside the flexible matrix, which could be attributed to the simplified manufacturing process of two-matrix composites. Indeed, our explorative study hints towards potentially significant manufacturing advantages of two-matrix composites, similar to what has been found in the research on pultrusion-stiffened hat stiffeners [8]. First, matrix migration *into* the micropultrusions is not necessary during the fabrication of two-matrix composites, allowing the impregnation stage to be expedited and inhibiting void formation. Second, the inherent bending stiffness of the micropultrusions facilitates micropultrusion alignment during manufacturing. Third, the use of micropultrusions enables us to take advantage of the characteristics of the pultrusion process: excellent fiber alignment (at least as good as high quality prepreg according to the manufacturer), high fiber volume fractions and control over the cross-sectional shape. As such, it can be expected that the average degree of fiber alignment is higher for the two-matrix composites as opposed to the single-matrix composites considered in this research, which would be beneficial in the context of compressive failure involving microbuckling/kinking.

### 3.2 Transverse tensile test

Transverse tensile testing (ASTM D3039) was performed on five UD specimens with the unflexibilized matrix and five UD specimens with the flexible baseline matrix, in order to obtain an indication of the transverse flexibility of both composites. Table 3 provides the

measured failure strains, stresses and transverse moduli for both categories. As expected, a higher failure strain is achieved for the composite with the flexible baseline matrix (1.19% versus 0.57% for the unflexibilized composite) and this could likely be increased when an even more flexible matrix is employed. Additionally, Table 3 shows a reduction in transverse tensile modulus for the composite with the flexibilized matrix (and a slight reduction in transverse tensile strength). Thus, the addition of the flexibilizing component indeed increases the transverse flexibility of the single-matrix composites. Although no transverse tests were performed on two-matrix composites in this research, a similar flexibilization effect is expected, based on the results of Vasiliev and Salov [6] and on the fact that the total transverse tensile strain of a two-matrix composite consists of the strain of the flexible matrix and the strain of the matrix inside the micropultrusions. Note, however, that the volume fraction of micropultrusions inside the flexible matrix is higher than the fiber volume fraction of the single-matrix specimens tested in transverse tension. Ultimately, tailoring the transverse flexibility of two-matrix composites would require balancing the flexibility of both matrix types and the volume fractions $V_b^c$ and $V_f^b$.

### 3.3 Single-matrix composites

The six single-matrix composite rings that were tested in the ring compression test all failed abruptly at a single location along their circumference, and showed a quasi-linear stress-strain behavior until failure (which was also observed in earlier work [16]). The rings with the unflexibilized matrix were characterized by a delaminated fracture zone (Figure 7a), which was attributed to the high energy release upon failure since no indications of premature delaminations could be observed in the stress-strain curves. Moreover, the delaminations were believed to be facilitated by the presence of inter-tow voids (shown before), reducing the interfacial strength between consecutive tow windings. The rings with the flexibilized matrix (Figure 7b) showed a non-delaminated, inclined fracture surface, which is indicative of failure

through fiber kinking. Fiber kinking is the typical failure mode for high $V_f$ UD carbon fiber/epoxy composites, and it is manifested through localized fiber buckling, matrix shear deformation, and the formation of a kink band (Figure 7c) [23]. As shown in Figure 7b, the inclination of the fracture surface with respect to the direction perpendicular to the fibers is approximately 23°, which is in line with typical kink band angles observed in literature [23]. The primary output parameter of the compression test was the ultimate compression strength, which is shown in Figure 7d for the six single-matrix composite rings. A significant strength difference could be observed between the rings with the stiff matrix (average $\bar{\sigma}_{c,1} = 635$ MPa) and those with the flexibilized matrix (average $\bar{\sigma}_{c,1} = 384$ MPa), with only a minor variation in strength values for the three rings in each category. This difference in compression strength between both ring types could be expected since a matrix with a lower stiffness typically provides less support to the fibers against buckling, and hence results in a lower fiber kinking strength [23]. The results from the ring compression test were also compared with those obtained from the CLC compression test using single-matrix composite rectangular specimens. Just like the composite rings, the rectangular specimens all failed abruptly during the compression test. Moreover, all rectangular specimens exhibited clear signs of fiber kinking failure, with a kink band extending through the width of the specimens at an angle of approximately 26° (see Figure 7e). Figure 7f displays the longitudinal compression strength values of the rectangular specimens, again showing a significant difference in compression strength between the specimens with the unflexibilized (average $\bar{\sigma}_{c,1} = 563$ MPa) and flexibilized (average $\bar{\sigma}_{c,1} = 367$ MPa) matrix. Comparing the average strength values from the CLC test with those of the ring test, it is clear that similar results were obtained. The values from the ring tests are slightly higher than those of the CLC test, likely due to the different manufacturing method, variations in fiber volume fraction, and the difference in test set-ups. Nonetheless, the strong similarities in terms of ultimate strength

and failure mode between the ring specimens and the CLC specimens supported further use of the ring compression set-up for evaluating the longitudinal compression strength of two-matrix composite specimens.

### 3.4 Two-matrix composites: failure modes

As mentioned before, nine types of two-matrix composite rings were tested in the compression set-up, all being different combinations of the three micropultrusion diameters (280 $\mu m$, 500 $\mu m$, and 700 $\mu m$) and the three flexibilized matrix systems (0.7 $MPa$, 1.4 $MPa$ and 1.7 $MPa$). Similar to the single-matrix composite rings, all two-matrix specimens failed abruptly at a single location along the circumference. However, different fracture types could be observed depending on the type of micropultrusions used. As shown in Figure 8a, the rings with 280 $\mu m$ diameter micropultrusions exhibited a clean, inclined fracture surface without delaminations or splitting. This was in stark contrast with the fracture zone of the rings with 700 $\mu m$ diameter micropultrusions, showing significant splitting and crushing of the two ends of the fracture zone (Figure 9a). The rings with 500 $\mu m$ diameter micropultrusions seemed to exhibit a mix of both failure types, combining splitting and inclined fracture surfaces.

#### 3.4.1 280 $\mu m$ diameter micropultrusions

Closer inspection of the 280 $\mu m$ specimens revealed that all fracture planes were inclined at an angle of $20 - 30°$ perpendicular to the fiber direction. Furthermore, after every test of a ring with 280 $\mu m$ diameter micropultrusions, small fragments originating from the fracture zone were observed in the test set-up. The specific angle of the fracture surfaces and the presence of these fragments suggested a specific failure mode for these composite rings: *micropultrusion kinking* inside the flexible matrix, as shown schematically in Figure 8b. Thus, the 280 $\mu m$ micropultrusions were believed to behave like individual fibers do in a typical composite and formed an inclined kink band under compressive loading, with the fragments

being remains of these kink bands (the fragments were typically one or two layers thick). For typical carbon fiber composites, kink band widths of 8-15 times the fiber diameter are stated in literature [24]. Likewise, the fragments for these two-matrix composites have a length of approximately 14 times the micropultrusion diameter. To further examine the hypothesis of micropultrusion kinking, optical and scanning electron microscopy (SEM) was performed on the fracture surfaces of these specimens. Figure 8c displays optical micrographs of inclined ring fracture surfaces. The micrographs show signs of fiber kinking within the individual micropultrusions, but only at one side of the micropultrusions. This observation of partial fiber kinking within the micropultrusions supports the hypothesis that the rings fail through micropultrusion kink band formation. When the micropultrusions form a kink band, one side of every micropultrusion is loaded in tension while the other side is loaded in compression (as schematically shown in Figure 8b). Since micropultrusions are composites themselves, it is likely that the compression side would fail through fiber kinking, as seems to be indicated in the micrographs. Figure 8c also provides a SEM micrograph (top view) of the fractured surface, on which the contours of a single micropultrusion are highlighted. Indeed, one half of the micropultrusion shows clear signs of fiber kinking, while the other half shows a fracture plane consistent with tensile failure. However, it must be noted that not all fracture surfaces inspected using SEM exhibited such clear examples of fiber kinking, since many of the fracture surfaces were severely damaged during the test procedure. Nevertheless, the combination of the abovementioned observations seems to support the hypothesis of micropultrusion kinking.

### 3.4.2 700 $\mu m$ diameter micropultrusions

The rings with 700 $\mu m$ diameter micropultrusions exhibited a crushing/splitting failure mode. In some specimens, this failure was situated at the circumferential position where the winding process was started, i.e. at the starting point of the micropultrusion (Figure 9b). This is

attributed to the micropultrusion misalignment at this point, which locally reduces compression strength. Since the number of windings required for a composite ring is inversely proportional to the micropultrusion diameter, a local micropultrusion misalignment has a much stronger impact for rings with larger diameter micropultrusions. Indeed, none of the ring specimens with $280\ \mu m$ micropultrusions failed at the winding starting point, while this was the case for several of the rings with $700\ \mu m$ micropultrusions. To further explore the failure of the rings with $700\ \mu m$ micropultrusions, we manufactured three rectangular specimens with the flexible baseline matrix ($E = 0.7$ GPa) using manual lay-up. These specimens were tested in the CLC compression set-up (ASTM D6641). One specimen failed through end-failure, and the other two specimens failed slightly outside the gauge section. While these failures are unacceptable for strength evaluation according to ASTM D6641, the two latter specimens could still provide some insight into the compression failure of the $700\ \mu m$ micropultrusions inside the flexible matrix. As shown in Figure 9c, the specimens did not show clear signs of micropultrusion kinking but rather exhibited crushing of the micropultrusions, as well as longitudinal splitting. The crushing of the individual micropultrusions is manifested as fiber kinking throughout the entire width of the micropultrusion. These microscopic observations seem to correspond to the crushing/splitting failure mode observed in the ring specimens with $700\ \mu m$ micropultrusions. The transition between kinking and splitting failure for larger micropultrusion diameters, has also been experimentally confirmed in earlier studies on conventional single-matrix composites with varying fiber diameter [25, 26]. This could be explained by the fact that the interfacial area (related to fiber-matrix adhesion) scales with the radius $r$, while the moment of inertia (related to bending stiffness) scales with $r^4$ [27]. Thus, it could be expected that the interfacial strength, governing the splitting strength, becomes critical for increasing micropultrusion

diameters. More (micro-scale) experiments are recommended to obtain conclusive evidence on failure mode transition in two-matrix composites.

### 3.5 Two-matrix composites: compression strength

Figure 10 provides the compression strength versus flexible matrix stiffness for the three types of micropultrusions that were used. In case of the rings with $280\ \mu m$ micropultrusions and a matrix stiffness of $E = 1.4$ GPa, one result was removed since an unrealistically high stress value was obtained, attributed to severe prior damage to the rubber loading ring. The results in Figure 10a for two-matrix composites with the smallest micropultrusions (left graph) seem to indicate a relation between compression strength and flexible matrix stiffness. For the most flexible matrix ($E = 0.7$ GPa) an average compression strength of $470$ MPa is obtained, which increases to $550$ MPa for the stiffest matrix ($E = 1.7$ GPa). This trend could again support the hypothesis of micropultrusion kinking, since a stiffer matrix could provide a higher support against buckling of the micropultrusions. However, other matrix features are also affecting the stability of the micropultrusions, thereby making it difficult to confirm the hypothesis of micropultrusion kinking on the basis of this data alone. Research on kinking failure of standard, single-matrix composites suggests that the matrix shear modulus and shear yield strength are also important, since kinking failure involves shearing deformation beyond the yield point [27]. As such, a high initial (shear) stiffness might be insignificant when the matrix has a very low shear yield strength, beyond which the shear stiffness is drastically reduced. Furthermore, the degree of adhesion between the flexible matrix and the micropultrusions could play an important role, as research on single-matrix composites has shown that the compression failure mode could change with changing interfacial strength [28]. An important remark here is that the interface in the case of two-matrix composites is likely a matrix-matrix interface, since the outside of the micropultrusions typically consists of

a thin matrix layer (see Figure 2). In any case, more detailed mechanical testing is recommended to establish the validity of the micropultrusion kinking hypothesis.

For the specimens with $500\ \mu m$ and $700\ \mu m$ micropultrusions (middle and right panes of Figure 10a respectively), it is not possible to observe a clear relation between compression strength and flexible matrix stiffness. This could be explained by the occurrence of a different failure mode, in particular for the $700\ \mu m$ micropultrusion specimens. Additionally, it is also clear that the variation in strength values increases for larger micropultrusion diameters. For example, the $280\ \mu m$ specimens show much smaller variation in strength values within each category than the $700\ \mu m$ specimens. This has been attributed to the higher overall quality and lower damage sensitivity that is achieved in specimens with smaller diameter micropultrusions. Compared to the $700\ \mu m$ specimens, those with $280\ \mu m$ micropultrusions had many more micropultrusions within the cross section, all densely packed. Consequently, a misalignment of a single micropultrusion would have a much less severe impact than in case of specimens with larger micropultrusions. It was not possible to identify a clear relationship between micropultrusion diameter and compression strength value, due to the substantial strength value variations for the specimens with larger micropultrusion diameters and due to the occurrence of different failure modes. Based on earlier results on conventional FRPCs, it can be expected that a larger micropultrusion diameter will result in a higher micropultrusion kinking stress, provided that this is the active failure mode [29]. Figure 10b combines all (non-normalized) results of the ring compression test, both on the single- and two-matrix composite rings. It is clear that the compression strength of all two-matrix composites is higher than that of the single-matrix composites with the flexible matrix. Thus, for the same matrix stiffness ($E_m = 0.7$ GPa), the two-matrix composites outperform their single-matrix counterparts, even with a lower overall fiber volume fraction. This is believed to be the consequence of the micropultrusion diameter (which is much larger than that of individual

fibers), the high fiber alignment within the micropultrusions and the high packing density of the two-matrix composites. On the other hand, the compression strength of all two-matrix composites remains below that of the single-matrix composites with the stiff matrix, which could be expected given the lower stiffness of the secondary matrix in the two-matrix composites. In Figure 10c, the strength results have been normalized by dividing by the fiber volume fractions ($V_f = 0.52$ for single-matrix composites and $V_f = 0.75 \cdot 0.60 = 0.45$ for two-matrix composties), effectively providing a measure of the "fiber efficiency". The figure shows that the two-matrix composites reach strength values well in the range of the single-matrix composites with the stiff matrix (Figure 10c). Additionally, Figure 10c again shows the large variation in strength values for the specimens with $700\mu m$ diameter micropultrusions, spanning almost the entire range of two-matrix composite strengths. While dividing the results by the corresponding $V_f$ could aid in the comparison between the single-and two-matrix composites, it is important to emphasize that two-matrix composites will typically always exhibit lower fiber volume fractions than single-matrix composites (Even if $V_b^c = V_f^b = 0.75$, the total fiber volume fraction, $V_f^c$, would be only 0.56).

### 3.6 Future outlook

#### 3.6.1 Recommendations for future work

The results of our proof-of-concept study on carbon fiber two-matrix composites continue along the line of those obtained in the original work of Vasiliev and Salov [6]. Nevertheless several recommendations for future research could be made. For example, the overall quality of the specimens could be improved, in particular for the specimens with the larger diameter micropultrusions, by employing a more accurate manufacturing set-up that offers better control over the individual micropultrusion alignment. Additionally, the constituent material properties should be optimized for use in two-matrix composites. It is recommended to increase the fiber volume fraction within the micropultrusions, to achieve higher strength of

the overall two-matrix composites. It would also be recommended to use the same matrix within all types of micropultrusions in future research (unless this is the parameter to be investigated), which was not practically possible in the current research. Furthermore, the use of other micropultrusion cross-sectional shapes should be investigated, as this could result in a higher compression strength [30] or could potentially offer a more uniform distribution of flexible matrix throughout the cross section of the two-matrix composites. In terms of the flexible matrix, it is advised to investigate matrices with an even lower stiffness, to truly leverage the potential of two-matrix composites. Moreover, different matrix materials (e.g. also thermoplastic matrices) or flexibilization techniques should be analyzed, taking into account the reduction in glass transition temperature that is typical for many flexibilized matrices. The ideal flexible matrix would enable simple processing techniques, adhere well to the micropultrusions, enable sufficient tailoring of the desirable stiffness and would have a glass transition temperature well outside the operating temperature range of the final composite (approximately -50°C to 70°C for aerospace composites). Finally, we recommend more detailed mechanical testing campaigns. For example, micro-scale compression testing of two-matrix composites could offer a deeper understanding of the failure mechanisms and the influencing factors, such as matrix shear properties, interfacial adhesion or micropultrusion diameter. In future tests, it is advised to include specimens consisting of micropultrusions embedded in the unflexibilized matrix and compare them with standard single-matrix specimens to investigate the influence of the manufacturing process variations. In addition to compression testing, it is also worthwhile to further analyze the behavior of two-matrix composites in other loading cases, such as longitudinal and transverse tension or shear, to further optimize the materials and manufacturing. These properties could also be tested on hoop-wound specimens, e.g. using the split disk method for longitudinal tension (ASTM D2290), axial loading of a hoop-wound cylinder for transverse tension (ASTM D5450), and

torsional loading of a hoop-wound cylinder for shear (ASTM D5448). Moreover, fatigue and impact testing could provide interesting insights, as the use of the flexible matrix might offer additional benefits for these loading types.

### 3.6.2 Potential applications

Based on our initial results, we believe that two-matrix composites could offer two primary advantages as opposed to standard composites: a higher degree of anisotropy and simplified manufacturing in terms of impregnation and fiber alignment. While Vasiliev and Salov originally introduced the two-matrix concept as an alternative for conventional UD layers in the development of composite structures [6], we expect it to be unlikely for this concept to radically replace the status-quo in composite applications, especially in applications where high fiber volume fractions are required. Indeed, one of the key limitations of two-matrix composites is their inherently lower $V_f$ (although our results show that the two-matrix composites can still outperform their single-matrix counterparts). Instead, we believe that two-matrix composites would be well suited for specific applications in which their primary advantages could be leveraged. For example, the combination of high transverse flexibility and high longitudinal strength and stiffness could be useful in the development of morphing wing skins that change shape during flight [11] or in helicopter flex beams that combine a high bending stiffness and a low torsional rigidity [9], i.e. applications where conventional composites cannot offer the combination of conflicting properties in different directions.

Moreover, we believe that the two-matrix concept could be useful for continuous carbon fiber 3D printing, in which micropultrusions are extruded and embedded into a secondary (not necessarily flexible) matrix. The first steps towards continuous-fiber 3D printing have recently been made using conventional carbon fibers and in-nozzle impregnation [31]. However, current approaches are challenging due to the limited control over the fiber waviness and impregnation, and since the fiber tows cannot be positioned in the vertical

direction. These challenges could be (partly) overcome by using micropultrusions instead of fiber tows, as they contain already aligned fibers, matrix material does not have to migrate into the fiber bundles, and the inherent stiffness of the micropultrusions could enable 3D reinforcement as well. Indeed, the potential for 3D printing of two-matrix composites has recently been demonstrated by others, after completion of this research [32].

## 4. CONCLUSIONS

In this research, we have developed, manufactured and tested a type of two-matrix composite, consisting of carbon fiber micropultrusions and flexibilized epoxy matrices, to further explore the feasibility of this unconventional material architecture. The blending of a standard epoxy resin with a flexibilizing component proved to be a suitable flexibilization strategy. However, future applications might require different approaches due to the strong reduction in $T_g$. Filament winding of two-matrix composite rings was found to be faster than the winding of equivalent single-matrix specimens, partly due to the simplified impregnation. Moreover, cross-sectional evaluation revealed a high micropultrusion packing density and the absence of voids in the flexible matrix. We therefore concluded the manufacturing benefits to be among the primary advantages of two-matrix composites. By using a radial compression test, we determined the longitudinal compression strength of the two-matrix composites and compared it to that of conventional single-matrix composites. Our results indicate that the failure mode of two-matrix composites depends on the micropultrusion diameter, being micropultrusion kinking for the smallest micropultrusions and splitting or crushing for the largest. Moreover, the most consistent results are obtained with the smallest diameter micropultrusions, which was attributed to the lower defect sensitivity. Based on our initial experiments, we concluded that two-matrix composites could offer higher compression strength than single-matrix composites with the same flexible matrix, despite the lower total fiber volume content.

However, we recognize that more detailed investigations into the micromechanics of two-matrix composites are recommended to fully uncover the failure characteristics and optimize the use of constituent materials. Nevertheless, we believe that the high anisotropy offered by two-matrix composites, as well as the manufacturing advantages in terms of fiber alignment and impregnation, could make the two-matrix concept an interesting paradigm towards more efficient composite structures.

## ACKNOWLEDGEMENTS

This research was entirely funded by the faculty of aerospace engineering at Delft University of Technology, The Netherlands. The authors are thankful to Maarten van Dijk from vDijk Pultrusion Products (DPP BV, The Netherlands) for supplying the micropultrusions used during this research and engaging in insightful discussions. The authors declare no competing interests.

## REFERENCES

[1] Vasiliev VV, Morozov EV. Mechanics of a Composite Layer. Advanced Mechanics of Composite Materials. 2nd ed. Amsterdam, The Netherlands: Elsevier; 2007.

[2] Soden PD, Hinton MJ, Kaddour AS. Chapter 2.1 - Lamina properties, lay-up configurations and loading conditions for a range of fibre reinforced composite laminates. Failure Criteria in Fibre-Reinforced-Polymer Composites. Oxford: Elsevier; 2004. p. 30-51.

[3] Zubillaga L, Turon A, Renart J, Costa J, Linde P. An experimental study on matrix crack induced delamination in composite laminates. Composite Structures. 2015;127:10-7.

[4] Abrate S. Matrix cracking in laminated composites: A review. Composites Engineering. 1991;1(6):337-53.

[5] Nairn JA. Matrix microcracking in composites. In: Talreja R, Månson J-AE, Kelly A, Zweben CH, editors. Polymer matrix composites. Amsterdam, The Netherlands: Pergamon; 2001. p. 403-32.

[6] Vasiliev VV, Salov VA. Development and examination of a two-matrix glass-fiber composite with high transverse strain. Mechanics of Composite Materials. 1985;20(4):463-7.

[7] Anderson T, Holzwarth R. Design and manufacture of Low-Cost Composite-Bonded Wing. 39th AIAA/ASME/ASCE/AHS/ASC Structures, Structural Dynamics, and Materials Conference and Exhibit 1998.

[8] Baker D, Rousseau C. Analysis and test of repair concepts for a carbon-rod reinforced laminate. 41st Structures, Structural Dynamics, and Materials Conference and Exhibit: American Institute of Aeronautics and Astronautics; 2000.

[9] Potter KD, Wisnom MR. Composites of extreme anisotropy Initial experiments. Plastics, Rubber and Composites. 2013;31(5):226-33.

[10] Cairns D, Bundy B. The Application of Pre-Cured Carbon Fiber/Epoxy Pultrusions as Reinforcement in Composite Wind Turbine Blades. 45th AIAA Aerospace Sciences Meeting and Exhibit 2007.

[11] Schmitz A, Horst P. Buckling of multiple discrete composite bundles in the elastomeric foundation of a curvature-morphing skin. Composite Structures. 2015;134:1014-23.

[12] Fleck NA. Compressive Failure of Fiber Composites. In: Hutchinson JW, Wu TY, editors. Advances in Applied Mechanics, Volume 33. Amsterdam, The Netherlands: Elsevier; 1997. p. 43-117.

[13] vDijk Pultrusion Products (DPP). The Product [JPEG].http://www.dpp-pultrusion.com/en/the-product-micro-pultrusion-products/. Last Accessed on: 09-02-2018.

[14] Brecher C, Emonts M, Schütte A, Brack A. Fiber-reinforced plastics enable new prospects for minimal invasive devices and interventions. Future Trends in Production Engineering: Springer; 2013. p. 297-305.

[15] Shaw S. Additives and modifiers for epoxy resins. In: Ellis B, editor. Chemistry and technology of epoxy resins. Dordrecht, The Netherlands: Springer Science + Business Media; 1993. p. 117-43.

[16] Kugler D, Moon TJ. A technique for compression testing of composite rings. Composites Part A: Applied Science and Manufacturing. 2002;33(4):507-14.

[17] Elkin R. Compression testing of NOL rings. Symposium on Standards for Filament-Wound Reinforced Plastics. Philadelphi, PA, USA: ASTM International; 1963.

[18] Kim RY, Tsai SW. A Compressive Test Method for Ring Specimens. In: Carillo G, Newell ED, Brown WD, Phelan P, editors. 33rd International SAMPE Symposium. Anaheim, USA 1988. p. 1159-68.

[19] Antonelli V, Decoster D, Marissen R, Beukers A. Improvements in the Pressure Distribution during the Forming of Thermoplastic Composites. International Journal of Material Forming. 2008;1(1):819-22.

[20] Lekhnitskii SG. Anisotropic Plates. New York, USA: Gordon and Breach Science Publishers; 1968.

[21] Halpin JC, Kardos JL. The Halpin-Tsai equations: a review. Polymer Engineering & Science. 1976;16(5):344-52.

[22] Cohen D. Influence of filament winding parameters on composite vessel quality and strength. Composites Part A: Applied Science and Manufacturing. 1997;28(12):1035-47.

[23] Schultheisz CR, Waas AM. Compressive failure of composites, part I: testing and micromechanical theories. Progress in Aerospace Sciences. 1996;32(1):1-42.

[24] Jumahat A, Soutis C, Jones F, Hodzic A. Fracture mechanisms and failure analysis of carbon fibre/toughened epoxy composites subjected to compressive loading. Composite structures. 2010;92(2):295-305.

[25] Yerramalli CS, Waas AM. A nondimensional number to classify composite compressive failure. Journal of applied mechanics. 2004;71(3):402-8.

[26] Lee S, Waas AM. Compressive response and failure of fiber reinforced unidirectional composites. International Journal of Fracture. 1999;100(3):275-306.

[27] Waas AM, Schultheisz CR. Compressive failure of composites, part II: experimental studies. Progress in Aerospace Sciences. 1996;32(1):43-78.

[28] Madhukar MS, Drzal LT. Fiber-matrix adhesion and its effect on composite mechanical properties. III. Longitudinal (0) compressive properties of graphite/epoxy composites. Journal of composite materials. 1992;26(3):310-33.

[29] Yerramalli CS, Waas AM. The effect of fiber diameter on the compressive strength of composites-A 3D finite element based study. Computer Modeling in Engineering and Sciences. 2004;6:1-16.

[30] Bond I, Hucker M, Weaver P, Bleay S, Haq S. Mechanical behaviour of circular and triangular glass fibres and their composites. Composites Science and Technology. 2002;62(7):1051-61.

[31] Matsuzaki R, Ueda M, Namiki M, Jeong T-K, Asahara H, Horiguchi K, et al. Three-dimensional printing of continuous-fiber composites by in-nozzle impregnation. Scientific reports. 2016;6:23058.

[32] Azarov A, Antonov F, Vasiliev V, Golubev M, Krasovskii D, Razin A, et al. Development of a two-matrix composite material fabricated by 3D printing. Polymer Science, Series D. 2017;10(1):87-90.

[33] Gamstedt EK, Sjögren BA. Micromechanisms in tension-compression fatigue of composite laminates containing transverse plies. Composites Science and Technology. 1999;59(2):167-78.

[34] Hexion. Epikote Resin 04908/Epikure Curing Agent 04908. Duisburg, Germany 2006.https://www.swiss-composite.ch/pdf/t-Hexion-Harz-EPR04908.pdf.

## FIGURE CAPTIONS

**Figure 1:** Single- and two-matrix composites. A) Schematic illustration of a 0/90° single-matrix composite laminate. Uniaxial tensile loading could result in transverse matrix cracking in the cross-plies, due to the anisotropy in failure strain of UD composite layers. Inset image was obtained from Ref. [33] B) Schematic illustration of the synthesis of a two-matrix composite: Fibers are first embedded in a stiff matrix and cured, resulting in composite bundles. These bundles are then embedded in a secondary, flexible matrix to create a two-matrix composite.

**Figure 2:** Carbon fiber micropultrusions. A) The three types of micropultrusions used during this research ($280\mu m$, $500\mu m$ and $700\mu m$ diameter) in straight configuration. Scale bar is 15mm B) The three types of micropultrusions in a bent configuration, showing that relatively high radii of curvature can be achieved. Scale bar is 15mm C) A cross-sectional micrograph of the smallest diameter micropultrusion, obtained with permission from Ref. [13]. Scale bar is $250\mu m$.

**Figure 3:** Experimental results of the flexibilized epoxy matrix. A) Flexural modulus of cured epoxy specimens as a function of relative flexibilizer content. Average of five specimens, error bars represent standard error. B) Two representative tensile stress-strain curves for the stiff (unflexibilized) epoxy matrix and the flexible baseline matrix (68% flexibilizer content).**Figure 4:** Manufacturing of compression testing specimens. A) Schematic illustration showing the dimensions of the thin-walled, hoop-wound ring specimens used for compression testing. B) Isometric view of the cylindrical mandrel with six slots on which the filament-wound ring specimens are manufactured and cured.

**Figure 5:** Compression testing of thin-walled rings. A) Schematic cross-sectional view of the compression test set-up. A rubber ring is placed around the composite ring and assembled in a steel base. The rubber ring is axially compressed, thereby transferring radial pressure to the composite ring, resulting in a hoop stress and radial stress component within the composite specimen. B) Example of radial and hoop stress variation throughout the wall thickness of a composite ring ($q = 20\ MPa$, $R_{in} = 0.1m$, $R_{out} = 0.104m$, $k = 4.82$). C) Ratio of hoop stress at inner wall to hoop stress at outer wall ($\sigma_{in}/\sigma_{out}$) versus ratio of inside to outside radius ($R_{in}/R_{out}$) for different values of ring anisotropy ($k$). The vertical dashed line indicates the radius ratio for the rings used during this research.

**Figure 6:** Cross-sectional micrographs of single-and two-matrix composites. A) Cross-section of a single-matrix composite, showing the presence of inter-two voids (black regions). B-C) Cross-section of a two-matrix composite with $500\mu m$ diameter micropultrusions, showing respectively a high (B) and locally lower (C) packing density. D-F) Cross-sections of two-matrix composites with respectively $280\mu m$, $500\mu m$, and $700\mu m$ diameter micropultrusions. All scale bars are $200\mu m$ unless otherwise indicated.

**Figure 7:** Compression testing of single-matrix composite rings. A) Delaminated fracture zone of composite ring specimen with the stiff matrix. Scale bar is 1mm. B) Inclined fracture zone of composite ring specimen with flexible baseline matrix. Scale bar is 1mm. C) Schematic illustration of kinking failure in UD composite loaded under compression. D) Compression strength results for the single-matrix rings with stiff matrix and flexible baseline matrix. Horizontal dashed lines indicate the average value. E) Close-up of the kink band in a rectangular UD specimen tested in longitudinal compression using the CLC set-up (ASTM D6641) Scale bar is 0.5mm. F) Compression strength results for the single-matrix UD, rectangular specimens with stiff and flexible matrices tested using the CLC set-up. Horizontal dashed line indicates the average value.

**Figure 8:** Micropultrusion kinking failure of two-matrix composite rings. A) Inclined fracture zones of the two-matrix composite rings with $280\mu m$ diameter micropultrusions. B) Schematic illustration of micropultrusion kinking inside the flexible matrix. The inset image shows the fragments that were visible after testing. Bending of the micropultrusions during kink band formation results in fiber kinking on the compression side. C) Optical (left and middle ) and SEM (right) micrographs of fracture surfaces showing fiber kinking on the compression side of the micropultrusions.

**Figure 9:** Compression failure of 700 $\mu m$ specimens A) Crushing/splitting fracture zones of the two-matrix composite rings with $700\mu m$ diameter micropultrusions. B) Close-up of two $700\mu m$-type rings that failed at the winding starting point. C) Micrographs of rectangular $700\mu m$-type two-matrix composite specimens tested in compression (CLC test), showing crushing of the micropultrusions, manifested as fiber kinking throughout the entire width of the micropultrusions (scalebars are 200 $\mu m$ and 2 mm for left and right figures respectively).

**Figure 10:** Compression strength results of the two-matrix composite rings. A) Compression strength versus flexible matrix stiffness for the specimens with $280\mu m$, $500\mu m$ and $700\mu m$ diameter micropultrusions respectively (from left to right). B) Compression strength versus matrix stiffness for the single-and two-matrix composite rings, non-normalized. C) Compression strength normalized by fiber volume fraction versus matrix stiffness for the single-and two-matrix composite rings, effectively providing a measure of "fiber efficiency".

## TABLE CAPTIONS

**Table 1:** Tensile testing results obtained by Vasiliev and Salov [1], for single-and two-matrix composites.

**Table 2**: Properties of the neat matrices used during this research, obtained using flexural and tensile testing, as well as DMA. For the flexural and tensile tests, the average of five (three in the case of the unflexibilized tensile test) specimens with one standard deviation is shown.

**Table 3**: Transverse tensile properties of the single-matrix composite specimens with the unflexibilized and the flexible baseline matrix. The average of five specimens with one standard deviation is shown.

**Figure 1**

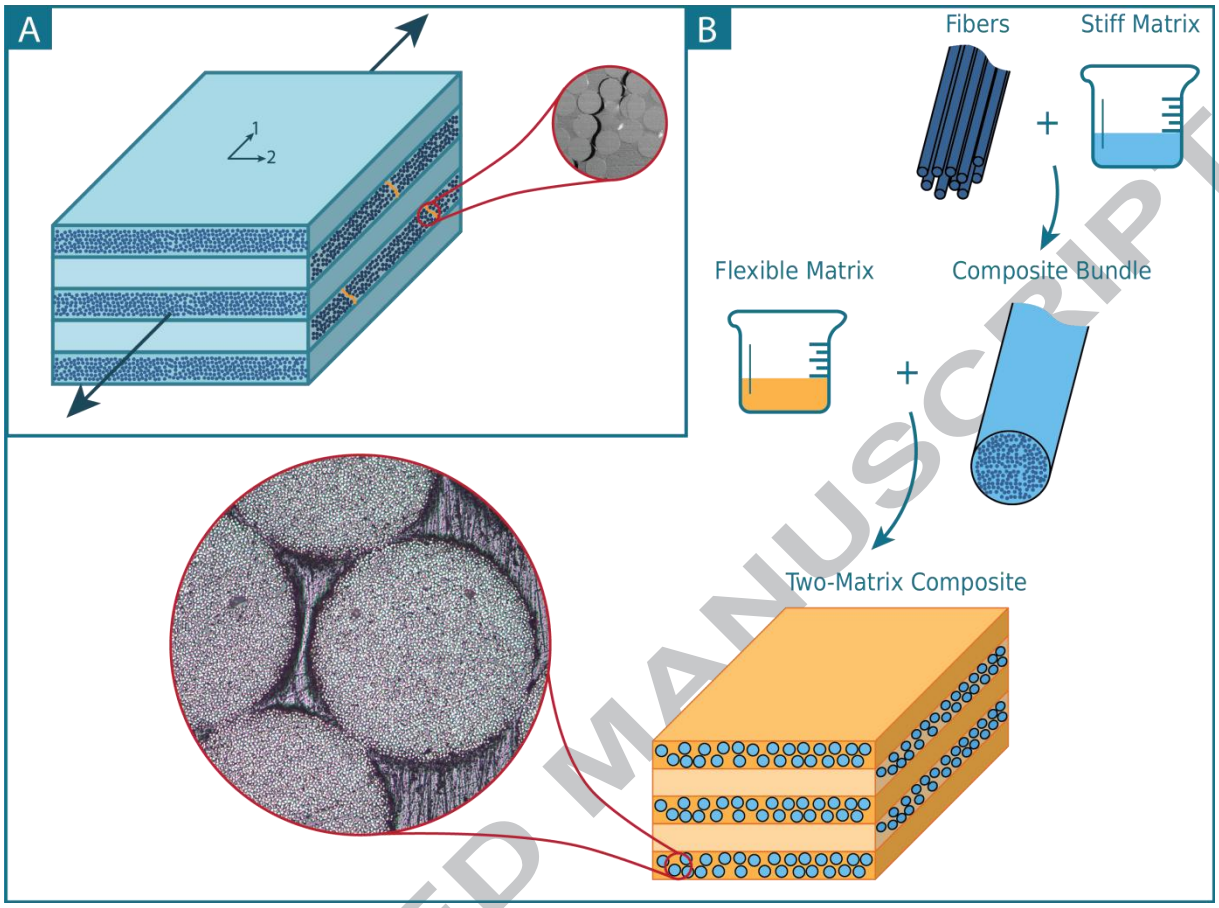


**Figure 2**

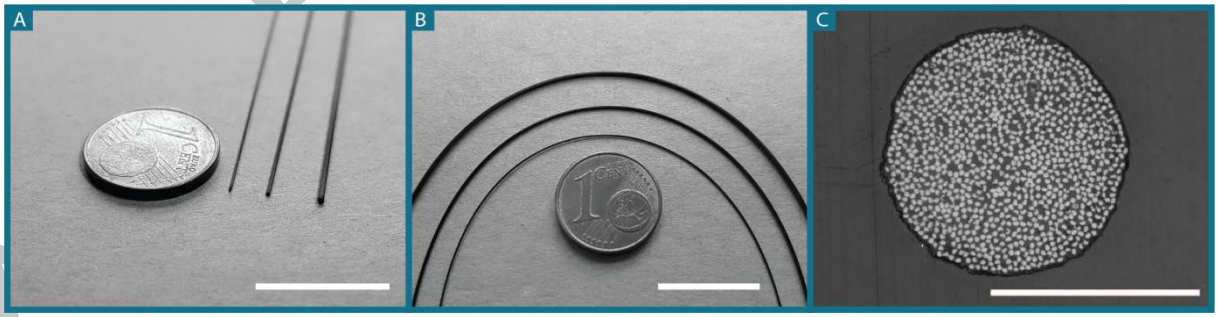

**Figure 3**

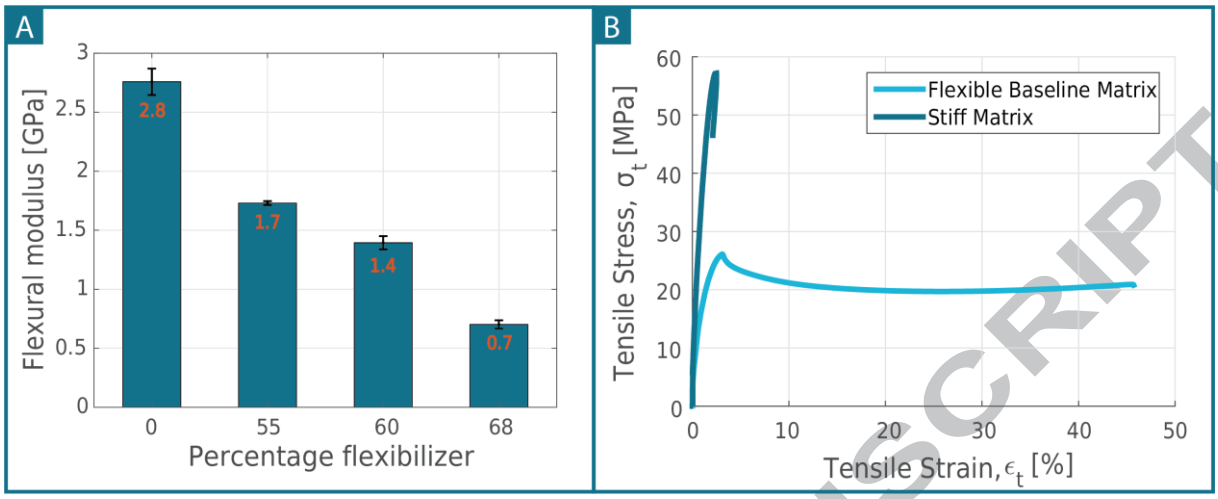


**Figure 4**

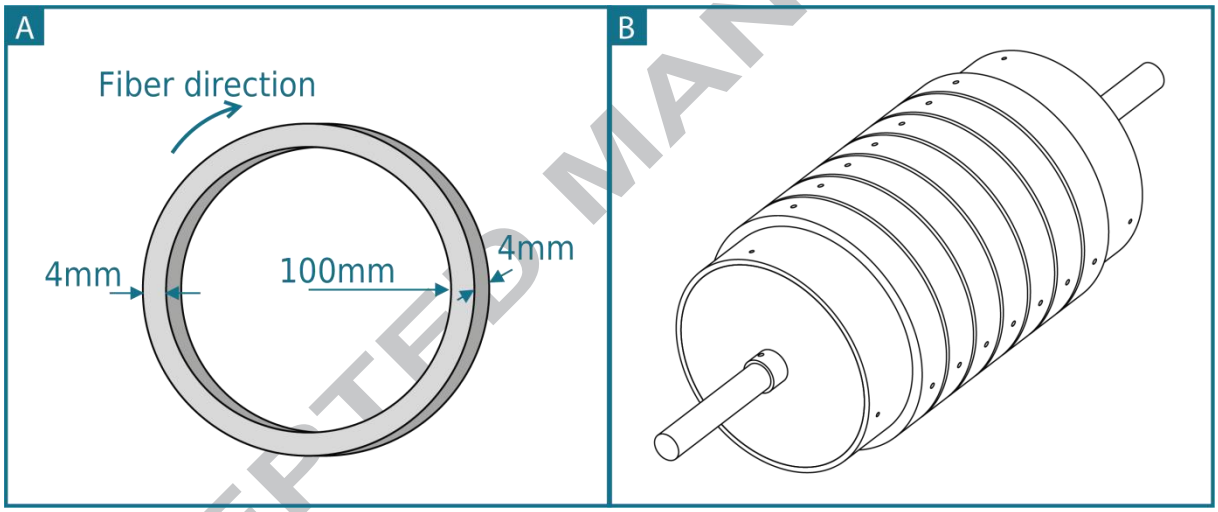

**Figure 5**

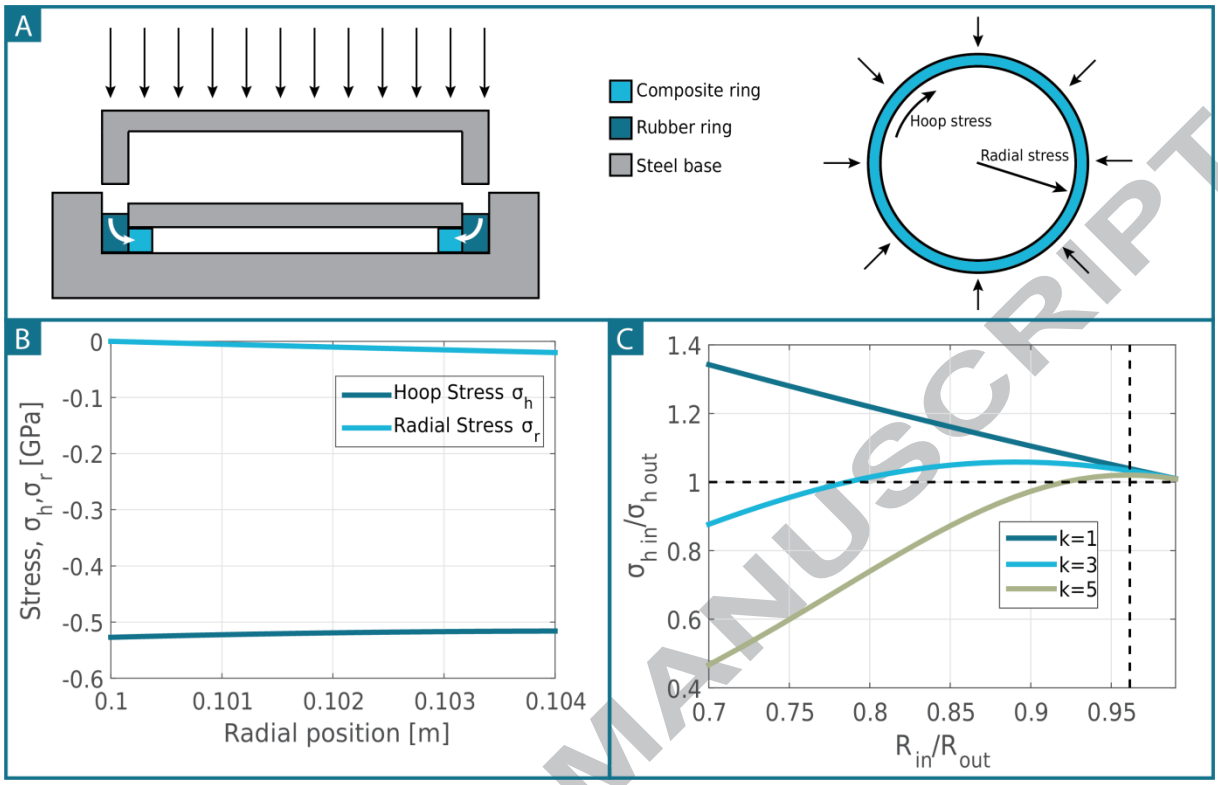


**Figure 6**

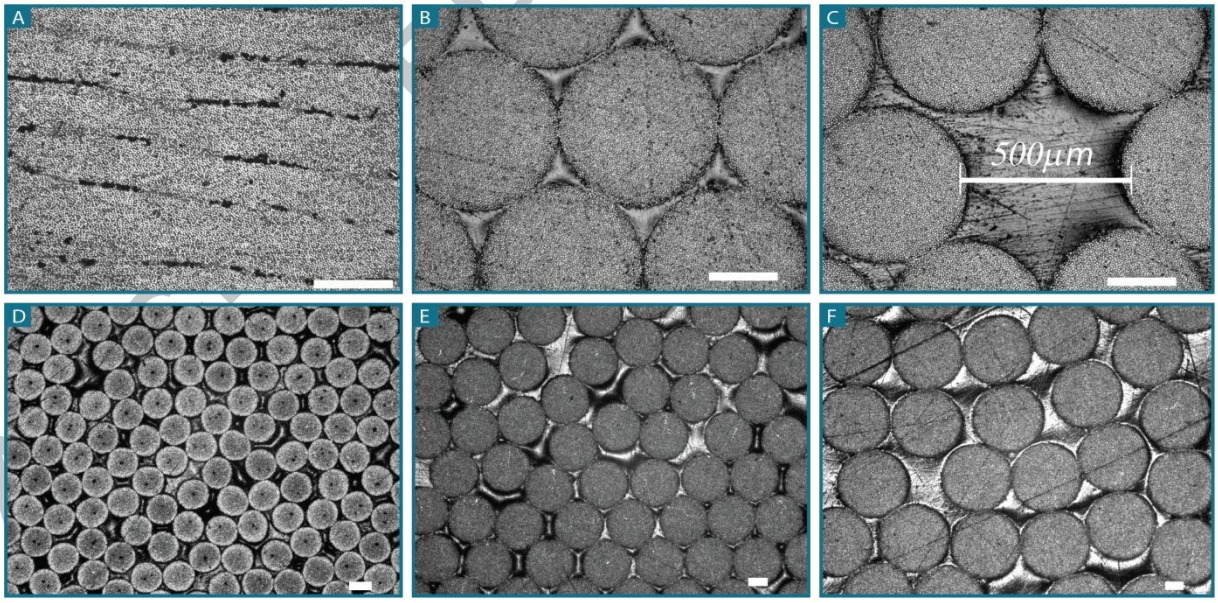

**Figure 7**

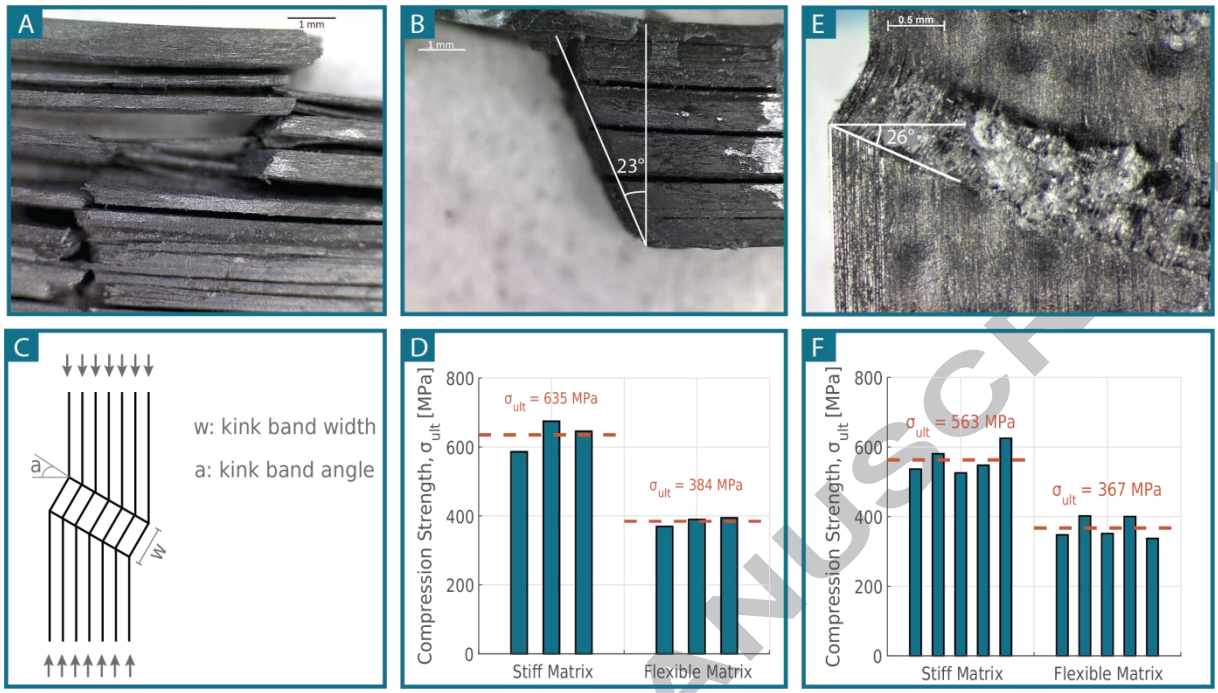


**Figure 8**

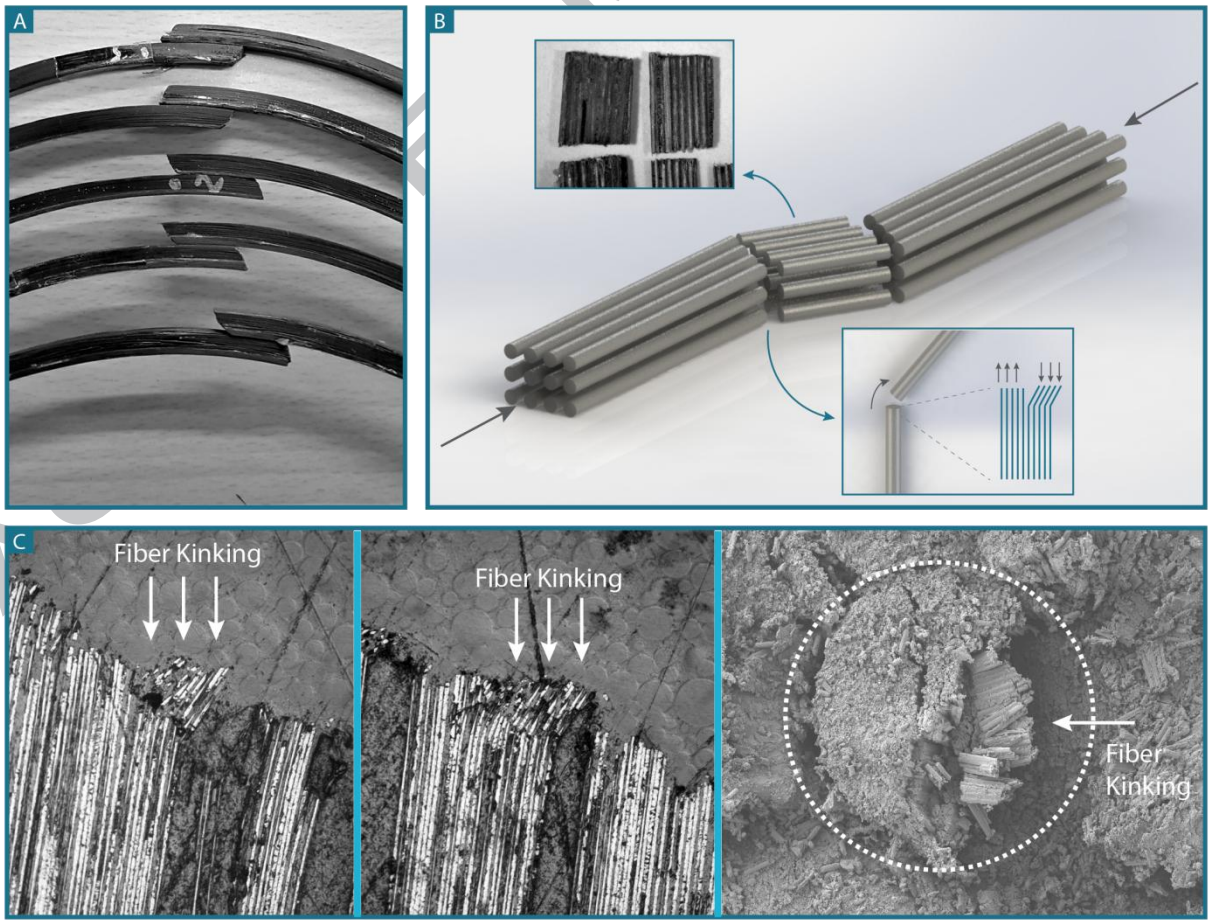


**Figure 9**

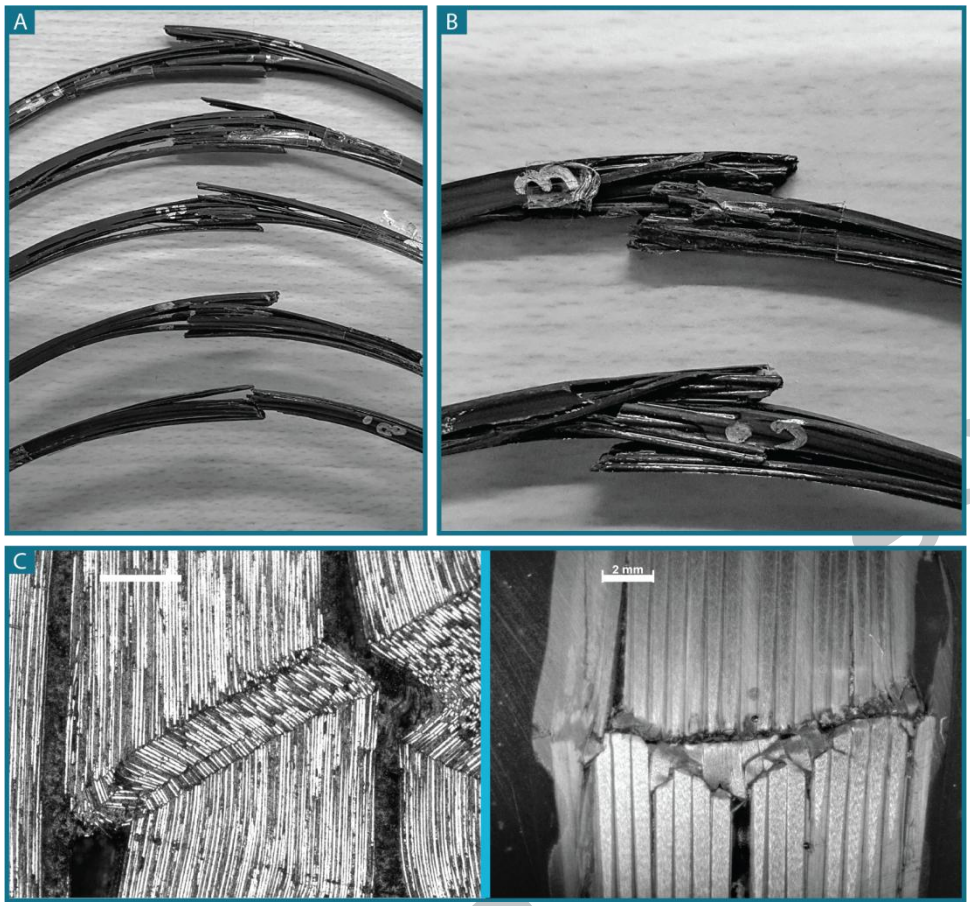
A
B
C
2 mm

**Figure 10**

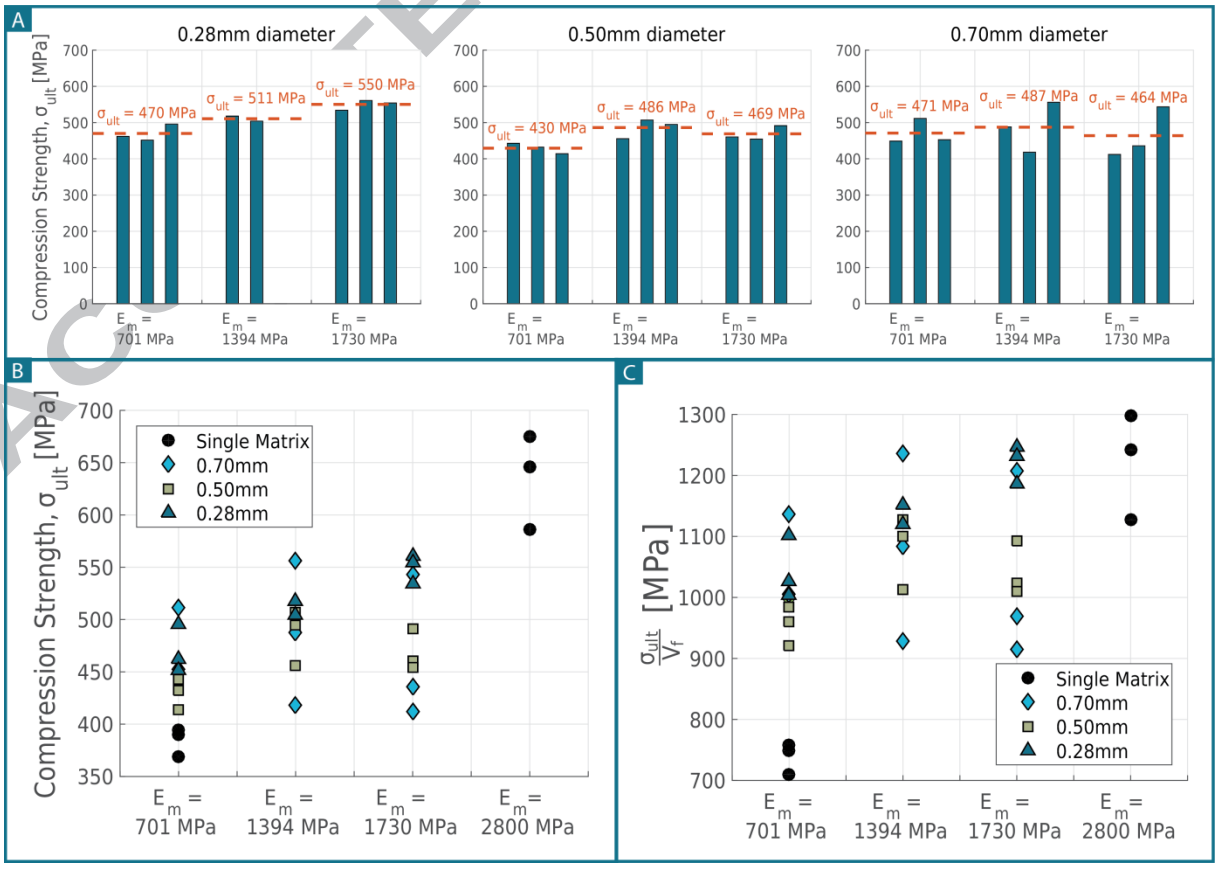
A
0.28mm diameter
0.50mm diameter
0.70mm diameter
Compression Strength, σult [MPa]
σult = 470 MPa
σult = 511 MPa
σult = 550 MPa
σult = 430 MPa
σult = 486 MPa
σult = 469 MPa
σult = 471 MPa
σult = 487 MPa
σult = 464 MPa
Em = 701 MPa
Em = 1394 MPa
Em = 1730 MPa
B
Compression Strength, σult [MPa]
Single Matrix
0.70mm
0.50mm
0.28mm
Em = 701 MPa
Em = 1394 MPa
Em = 1730 MPa
Em = 2800 MPa
C
σult / Vf [MPa]
Single Matrix
0.70mm
0.50mm
0.28mm
Em = 701 MPa
Em = 1394 MPa
Em = 1730 MPa
Em = 2800 MPa

**Table 1**

| Composite type | Fiber Volume Fraction | Tensile Strength (MPa) | Tensile Failure Strain (%) |
|---|---|---|---|
| Single-matrix: glass fibers + stiff matrix | 0.67 | 1470 | 0.2 |
| Single-matrix: glass fibers + flexible matrix | 0.65 | 1100 | 1.2 |
| Two-matrix: glass fibers + flexible and stiff matrix | 0.51 | 1420 | 3.0 |

**Table 2**

| Matrix type | Flexibilizer content (%) | Flexural modulus (GPa) | Tensile failure strain (%) | Glass transition temperature (°C) |
|---|---|---|---|---|
| Flexible baseline | 68 | 0.7 +/- 0.13 | 35.4 +/- 9.9 | 37 (peak of E")<br>57 (peak of tan($\delta$)) |
| Flexible type 2 | 60 | 1.4 +/- 0.11 | - | - |
| Flexible type 3 | 55 | 1.7 +/- 0.03 | - | - |
| Unflexibilized | 0 | 2.8 +/- 0.22 | 2.14 +/- 0.02 | 82 [34] |

**Table 3**

| Matrix type | Transverse tensile failure strain (%) | Transverse tensile failure stress (MPa) | Transverse tensile modulus (GPa) |
|---|---|---|---|
| Unflexibilized | 0.57 +/- 0.09 | 39.02 +/- 3.40 | 6.28 +/- 0.32 |
| Flexible baseline | 1.19 +/- 0.21 | 32.90 +/- 3.98 | 4.12 +/- 0.73 |